1.2 On the Structure and Chemistry of Complex Oxide Nanofeatures in Nanostructured Ferritic Alloy U14YWT

— D. Bhattacharyya, P. Dickerson, S. A. Maloy, A. Misra, M. A. Nastasi *(Los Alamos National Laboratory)* and G. R. Odette *(University of California Santa Barbara)*

OBJECTIVE

The objective of this work is to characterize the different types of precipitates in a UCSB model nanostructured ferritic alloy U14YWT, in the hot-isostatically pressed condition, in order to understand their distribution, morphology, chemical composition and crystal structure.

SUMMARY

The remarkable radiation damage resistance of nanostructured Ferritic alloys (NFAs) is attributed to the large numbers of matrix nano-features (NFs) of various types, which can enhance the recombination of displacement defects and trap transmutant helium in fine scale bubbles. Conventional and high resolution transmission electron microscopy and energy dispersive spectroscopy were used to characterize the various types of NF and larger oxide phases in a model 14Cr-3W-0.4Ti-0.25Y_2O_3 NFA (14YWT) Hot Isostatic Pressed (HIP-ed) at 1150°C. Large $CrTiO_3$ precipitates (50-300 nm) and small diffracting NFs (< 5 nm) were found in this alloy. One major new result is the observation of an additional type of nano-feature (10-50 nm), orthorhombic in structure, with a square center cross section, that constitutes a new kind of Y-Ti oxide phase with lattice parameters different from those of known Y and Ti complex oxides. The interfaces of these particles seem to be semicoherent, while manifesting a possible orientation relationship with the BCC matrix. The ratio of Y to Ti varies between < 1 and 2 for these larger NFs.

BACKGROUND

The compelling need to reduce mankind's reliance on fossil fuels and the consequent deleterious effects on the environment, while meeting a rapidly growing demand for energy has generated a worldwide interest in advanced fission and fusion energy [1-2]. The viability of nuclear energy systems will ultimately depend on developing new high performance structural materials that can provide extended life under extremely hostile conditions, characterized by combinations of high temperatures, large time varying stresses, chemically aggressive environments and intense neutron radiation fields [1, 3]. The lifetime goals for some reactor components will require tolerance of up to 400 displacements-per-atom (dpa). Displacement damage produces excess concentrations of defects consisting of vacancies and self-interstitial atoms (SIAs). Neutron irradiation also generates a wide range of transmutation products, most notably insoluble helium. These sources of primary damage interact to drive complex microstructural, dimensional and microchemical evolutions, which in turn typically degrade a host of performance-sustaining material properties [1, 3-4]. Complex irradiation effects depend on the *combination* of the irradiation temperature, dpa, dpa rate and He/dpa ratio, as well as the composition and starting microstructure of the material.

We focus here on potentially transformational nanostructured ferritic alloys (NFAs) that show promise of meeting many of these challenges. Note that NFAs derive from earlier

roots in oxide dispersion strengthened (ODS) steels (an example is PM2000 [5]). As discussed in recent review articles [3, 6] and the references contained therein, NFAs manifest high tensile, creep and fatigue strengths, unique thermal stability and show a remarkable tolerance to neutron irradiation. The outstanding characteristics of NFAs derive primarily from the presence of a high density of nm-scale Y-Ti-O rich nanofeatures (NFs) that range in size from ≈ 1 to 50 nm. The NFs enhance SIA-vacancy recombination; and, perhaps most importantly, trap helium in small, high-pressure gas bubbles [7]. These bubbles reduce the amount of helium reaching grain boundaries, thus mitigating toughness loss at lower temperatures, and potential degradation of creep rupture properties at higher temperature. In principle, helium trapped in a high concentration of extremely small bubbles also reduces all other manifestations of radiation damage, including void swelling, that occur in other alloys [3, 6-8]. Another great advantage of having the NFs dispersed in the Fe matrix is that they impede dislocation climb and glide, and thus improve their strength and creep resistance. The high creep strength of these materials allows their use at high temperatures above the displacement damage regime. The effect of a high density of Y-Ti-O rich nano-clusters on the high temperature strength of ferritic alloys was studied in detail by Hoelzer, Miller et al [9] and it was shown that nano-clusters improved the high-temperature strength of these alloys significantly. These nano-features were found to be extremely stable with respect to temperature, and they were present in a high number density even after 24 hrs at 1300 °C in 12YWT, 14YWT and MA957 in atom-probe studies by Miller et al. [10].

NFAs are typically processed by ball milling pre-alloyed rapidly solidified metal and yttria (Y_2O_3) powders [3]. Proper milling effectively dissolves the Ti, Y and O solutes that then precipitate as NFs during hot consolidation by extrusion, or hot isostatic pressing (HIPing). Powder consolidation is usually followed by a series of deformation processing steps. Various studies have shown that there is not a single type of NF, but rather what might best be described as an NF zoo, even in a single alloy, like MA957 [3, 6]. The detailed characteristics of the NFs vary even more from alloy to alloy, since they are very sensitive to composition and processing variables. For example, the number density and volume fraction of NFs increase, while their sizes decrease, at higher consolidation temperatures [3, 6, 11]. Further, Ti is needed to form small NFs at higher consolidation temperatures [11]. Thus one critical objective is identifying the structure, composition and interface structures, that is the 'character', of various NFs. Such information is crucial to the development of a knowledge base for alloy optimization. A substantial body of work exists on the characterization of these NFs using atom probe tomography (APT) – see, e.g., [12-13]

It is the authors' view that the ability of NFs to trap and form fine scale He bubbles is expected to depend not only on their number densities and size distributions, but also on their interfacial and elastic properties. In particular, recent experiments and atomistic models have shown that the geometry and the atomic structure of interfaces play an important role in improving the radiation tolerance of materials [14-16]. It is crucial to understand the crystal structure, crystallography and interface properties of all nano-scale oxides in ODS-steels as opposed to focusing only on the 2-5 nm particles and ignoring everything else in the microstructure. It is conceivable that the 20 nm particles may have an interface structure that may be a stronger sink for defects than the 2-5 nm particles. The only way to know this is to understand in detail all the particles and then in future work, model the structure of the interfaces and their sink strength. Some recent TEM characterization of nano-scale precipitates in ferritic steels of somewhat different

composition than that in the present work has been done by Klimiankou et al. [17-18], which demonstrates the effect of larger particles on inert gas entrapment. In this paper, the authors show that there are three types of NFs in a model Fe-14Cr-3W-0.4Ti-0.25Y_2O_3 alloy (called U14YWT) that was HIPed at 1150°C. The structure and chemistry of these three types of NFs are characterized using various TEM techniques, with particular focus on the 10-50 nm sized nano-feature class, which exhibits a hitherto unobserved crystal structure for such precipitates.

EXPERIMENTAL METHODS

Materials

U14YWT was prepared at UCSB by mechanically alloying atomized powders of Fe - 14 wt% Cr - 3 wt% W - 0.4 wt% Ti with 0.25 wt% Y_2O_3 in a ball mill attritor at ambient temperature for 10 hrs in a dry Ar atmosphere [11, 19]. The milled powder were then vacuum degassed and canned prior to hot isostatic pressing (HIPing) to full consolidation at 1150°C and 200 MPa for 3 h. This U14YWT is part of a much larger matrix of model alloys issued to study NFs and NF thermokinetics using a variety of characterization techniques [3, 11, 19].

Transmission Electron Microscopy (TEM)

In this work TEM specimens were prepared using a dual beam focused ion beam (FIB) FEI DB235™ instrument. Low energies down to 10 keV were used to perform final polishing of the sample, with very low currents (500 pA). In some instances, the FIB-ed sample was thinned further using a Gatan® PIPS™ precision ion mill at 2 keV. Subsequently, the samples were cleaned using a plasma cleaner with Ar gas.

The FIB-ed samples were then examined using an FEI Tecnai F30™ TEM operated at 300 kV. Energy dispersive X-ray spectroscopy (EDS) was used to measure the composition of the precipitates in the scanning transmission (STEM) mode. A relatively small spot size (no. 6) and a strong gun lens condition (no. 6) were maintained during STEM imaging and analysis. During collection of each spectrum, special care was taken to obtain enough counts so that the “peak to background ratio” was reasonably high for each of the relevant peaks. The collection times used were 30-60 s for each precipitate. The FEI™ software “TIA” was used to quantify the elements in EDS spectra. The background was calculated and subtracted automatically by the software. The uncertainties in the chemical composition of the precipitates presented in the tables are less than ± 5% of the value of the measured concentration of any given species.

High-resolution TEM (HRTEM) images were analyzed using Gatan® Digital Micrograph™ and NIH’s ImageJ™ software.

RESULTS

Three distinctly different kinds of features were observed, which could be categorized into the following classes: (a) large faceted, but irregular shaped features, 50-300nm in size; (b) intermediate sized 20-50 nm NFs with square center cross sections; and (c) small 2-5 nm NFs which appear to be round. Note, while we have classified the intermediate sized phases as NF in this paper, some literature restricts NF sizes to < 5-10 nm. It is the structure, chemistry and matrix-particle orientation relationship (OR) of

the oxide phases, with special emphasis on the intermediate sized phase, that we focus on and present in this paper.

Large, faceted features (50-300nm)

The high angle annular dark field (HAADF) image in Fig. 1 shows a region of the

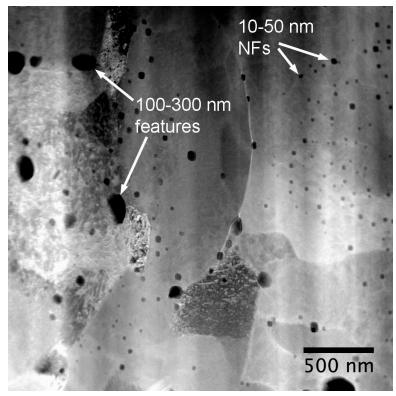

Fig. 1. HAADF STEM image showing large and intermediate sized particles.

FBI-sectioned TEM specimen. Many grains of various sizes are visible, ranging from 250nm-1mm, with a large number of dark particles distributed both inside the grains and on the grain boundaries. The dark contrast of these features suggests that they contain large amounts of oxygen, and therefore have a lower average Z than the Fe matrix. The presence of oxygen is also apparent in the EDS results presented below. Spot and EDS scan composition measurements were performed on some of the 100-300nm features, which were mostly located on the grain boundaries.

The EDS spectrum from one of these large features, presented in Fig. 2(a), shows high intensities of the Ti(K), Cr(K) and O(K) peaks, along with a weak Fe(K) peak, that is likely due to a thin layer of Fe matrix above or below the particle. The chemical concentrations of different elements obtained from spot spectra for 7 such large features, presented in Table 1, show average compositions of ≈ 20 at. % Cr and Ti and, nominally, ≈ 60 at % O and trace quantities of Fe, W and Y.

Table 1. Chemical composition (in atomic %) of 7 large faceted particles in the 100-300 nm size showing the presence of almost equal amounts of Ti and Cr.

	1	2	3	4	5	6	7	Average
O(K)	48.1	61.6	53.9	65.8	61.32	62.67	65.89	59.90
Ti(K)	27.2	20.6	23.8	18.1	20.4	19.84	17.76	21.10
Cr(K)	24.2	17.6	21.9	15.9	18.11	14.97	16.19	18.41
Fe(K)	0.3	0.2	0.3	0.2	0.15	0.2	0.14	0.21
Y(K)	0	0	0	0	0	2.29	0	0.33
W(L)	0.06	0	0	0	0	0	0	0.01

The trace of a line EDS scan on one such feature is shown in Fig. 2(b), and the elemental profile of Fe is shown in Fig. 2(c), and those of Ti, Cr and O are shown in Fig. 2(d). The drastic drop in the Fe(K) peak intensity suggests that the particle occupies most of the thickness of the sample and that there is hardly any Fe inside the particle. Since the particle is about 140-160 nm wide in the direction of the trace, and since the shape of the particle is almost equiaxed, it may be assumed that the feature occupies most, if not all, of the thickness of the sample. Hence the X-ray peaks obtained from the region of the feature arise predominantly from the elements in the feature, and not from the matrix and any Fe in the EDX spectrum comes from a very thin layer of Fe matrix above or below the oxide. The intensities of the Ti(K) and Cr(K) peaks are almost equal inside the feature. Note that the Cr content of the particle is only slightly higher than the 14 % Cr in the FeCr matrix. However, if the feature did not contain Cr, some level of depletion would be observed.

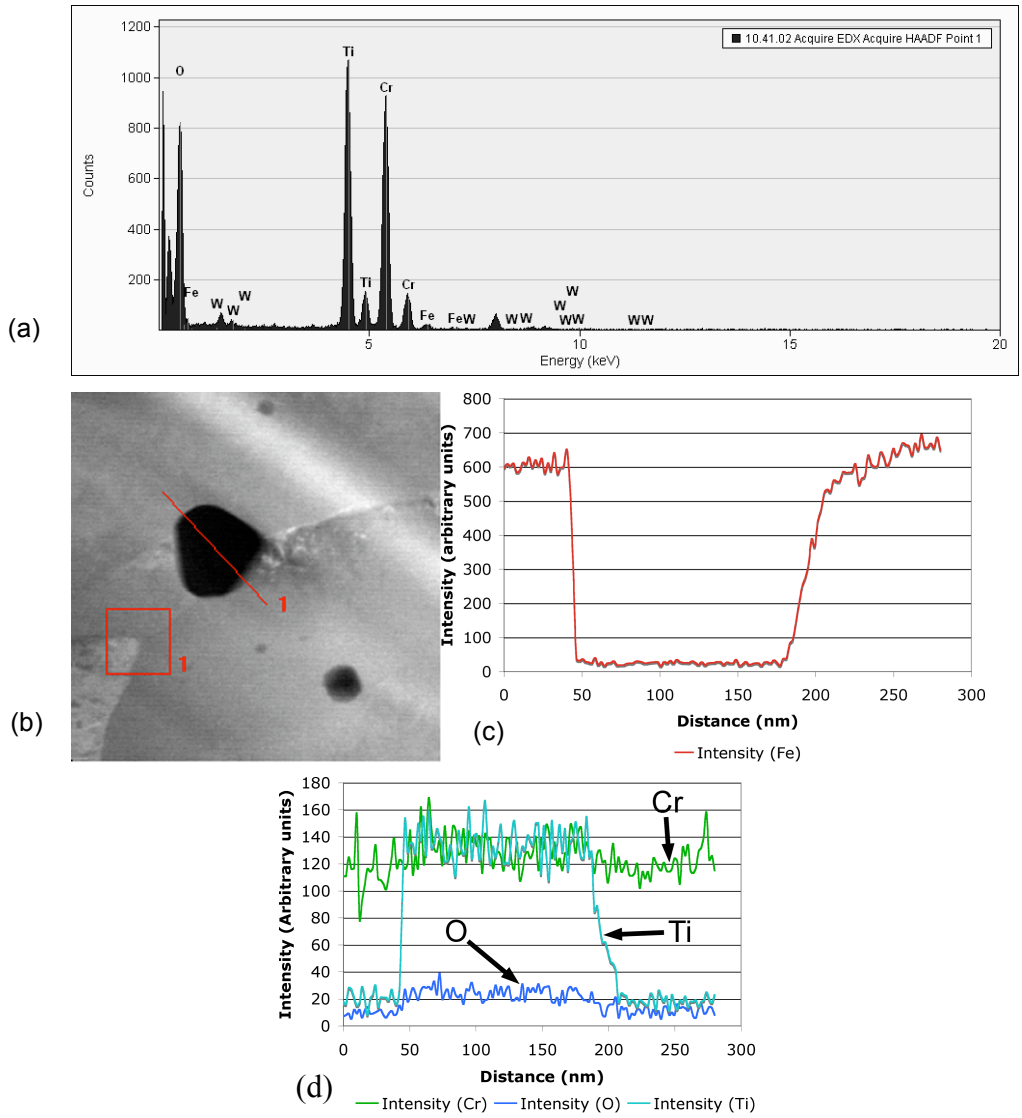

Fig. 2. (a) EDS spectrum collected from a spot in a large faceted particle showing mainly Ti, Cr and O peaks, apart from the Fe peak from the matrix, (b) A line spectrum

trace across one such particle, (c) The drift-corrected spectrum profile along the trace shown across the particle in (b) showing a drastic drop of the Fe intensity inside the particle, and (d) Almost equal intensities of Ti (K) and Cr(K) peaks and a rise in the O(K) intensity in the particle.

The structure of the large features was determined by BF TEM imaging and selected area diffraction. A BF TEM image of one feature is shown in Fig. 3(a), with the BCC Fe matrix on a [001] zone axis (ZA). The corresponding selected area diffraction pattern (SADP) is shown in Fig. 3(b). It is clear from the BF TEM image and the SADP that two of the major facets of the particle are parallel, or almost parallel, to {200} Fe (BCC) planes. The other facets are also parallel to BCC low index planes. The SADP in Fig. 3(b) also shows many spots from the precipitate, that were used to measure the d-spacing values shown in Table 2, along with those reported in the literature for a rhombohedral structure [20]. It is clear that there is reasonable agreement between the two sets of observations.

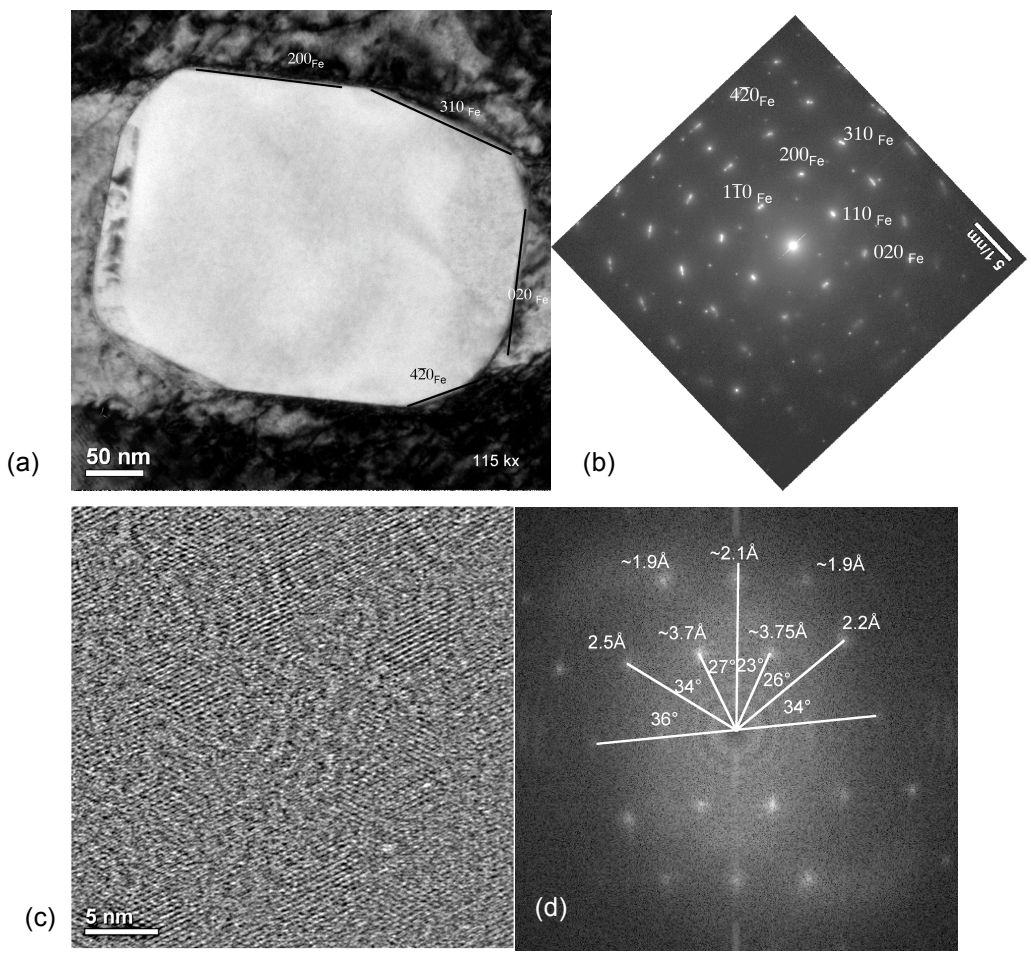

Fig. 3. (a) BF TEM image of a big faceted precipitate with the Fe matrix on a 001 zone axis, (b) Corresponding selected area diffraction pattern showing both matrix and precipitate spots, (c) HRTEM image of the particle shown in (a), and (d) FFT of the HRTEM image shown in (c) showing a few spots d-spacing equal to or close to $CrTiO_3$ as reported in the literature.

Table 2. *d-spacing values of different planes of $CrTiO_3$ as measured and as reported in the literature* [20]

	Measured (Å)	Reported in literature (Å)
1	3.7 - 3.8	3.67
2	2.0 - 2.2	2.2
3	1.9	1.835

An HRTEM image of the particle is shown in Fig. 3(c) and the corresponding fast Fourier transform (FFT) is presented in Fig. 3(d). The d-spacing values of the phase comprising the particle as measured from this FFT image agree with those measured from the SADP shown in Fig. 3(b). Therefore, the feature in Fig. 3(a) is consistent with rhombohedral $CrTiO_3$, although a precision measurement of lattice parameters was not performed.

Intermediate sized square NFs (10-50 nm)

Intermediate sized square-shaped NFs were also observed in the sample, as seen in the HAADF micrograph in Fig. 1. A higher magnification image of some similar particles is shown in Fig. 4(a). It is clearly visible in this image and in the images in Fig. 4(b) and 4(c), which show other ferrite grains, that these particles have a nominally square cross-section, and that they are morphologically oriented in the same direction inside any given grain. These precipitates will be referred to here as “large NFs”. The area fraction of these nominally square shaped large NFs varies from 1 to 4% from grain to grain, which is equivalent to a volume fraction of 0.15-0.8%, assuming a roughly cubic shape. The number density of these particles was found to vary between $2x10^{20}$ and $7x10^{20}$ NFs/ cubic m, and the surface area per unit volume was calculated to be in the vicinity of $8x10^5$ – $2.4x10^6$ m^2/ m^3.

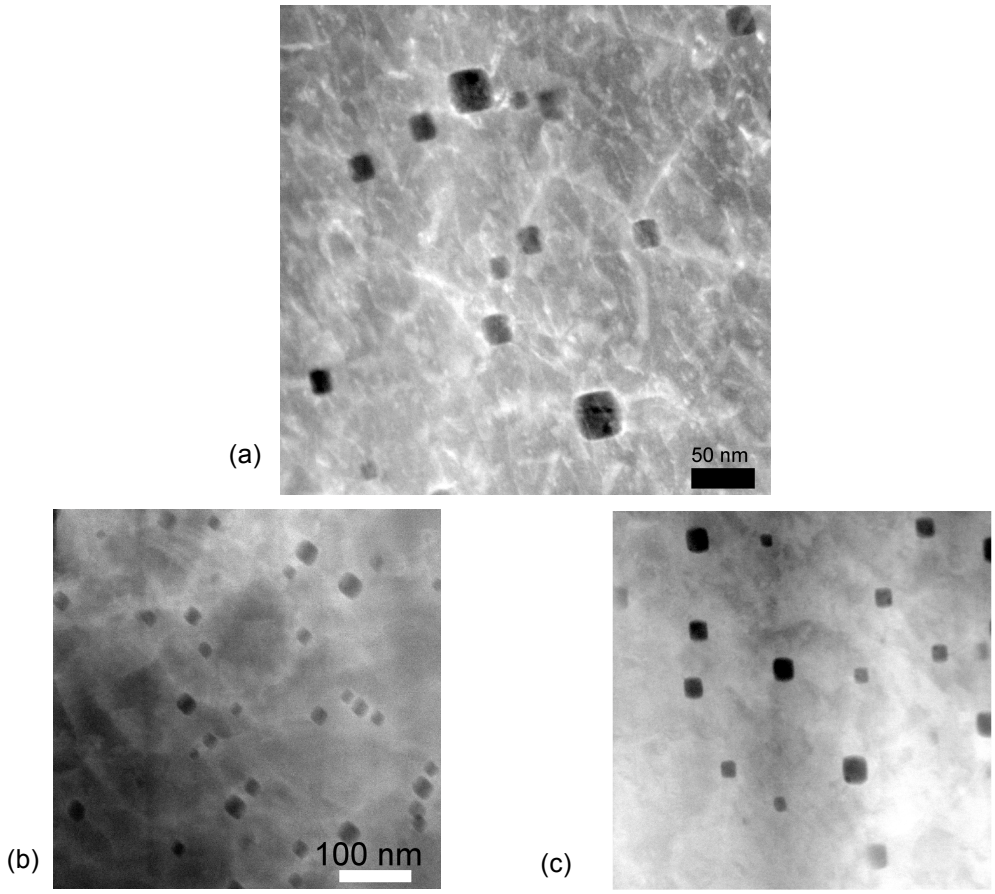

Fig. 4. (a) STEM HAADF image of 10-50 nm precipitates or "larger NFs" with a square shape in cross-section, mostly located on dislocations, (b) and (c) show similar precipitates or "nano-features" in other ferrite grains, all oriented with their facets parallel inside any given grain.

The STEM image in Fig. 5(a) shows one of the largest NFs in this class (indicated by arrow). There are four main facets which give the nano-feature an approximately square shape. The corners have smaller facets or are rounded, implying that these NFs are not strictly square, but are polygonal with a roughly square shape in their center plane. The EDS spectrum in Fig. 5(b) was collected from the particle showed in Fig. 5(a). The spectrum shows intense peaks for Y, Ti and O, along with weaker peaks from Fe and Cr; the latter arise most likely from matrix located above or below the NF, since the 50-60nm NF is probably smaller than the foil thickness in this area. A profile of the Fe-K and Cr-K peak intensities (Fig. 5(c)) shows a sharp drop for both Fe and Cr inside the NF, suggesting that any Cr signals arise from the matrix, unlike in the case of the larger particles, where the Cr intensity remains the same while the Fe intensity decreases. The Ti, Y and O intensities increase significantly inside the NF, while the small W intensity decreases to almost zero, as shown in Fig. 5(d). Other similar, but smaller, NFs also showed the same type of concentration profiles. Thus it can be stated with considerable certainty that these NFs are comprised mainly of Ti, Y and O. The HAADF image in Fig. 5(e) shows four such features, with sizes varying from ~25-60nm. The Y and Ti content, and the Y/Ti ratio are shown in Table 3.

(a)

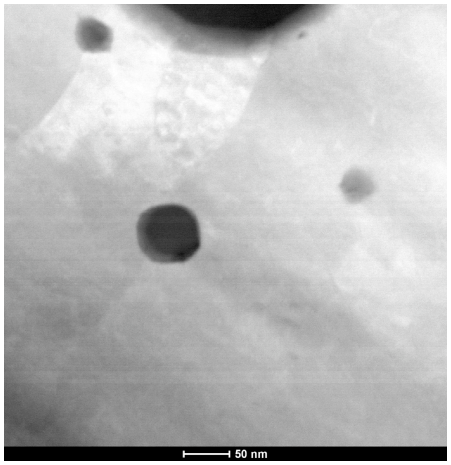
50 nm

(b)

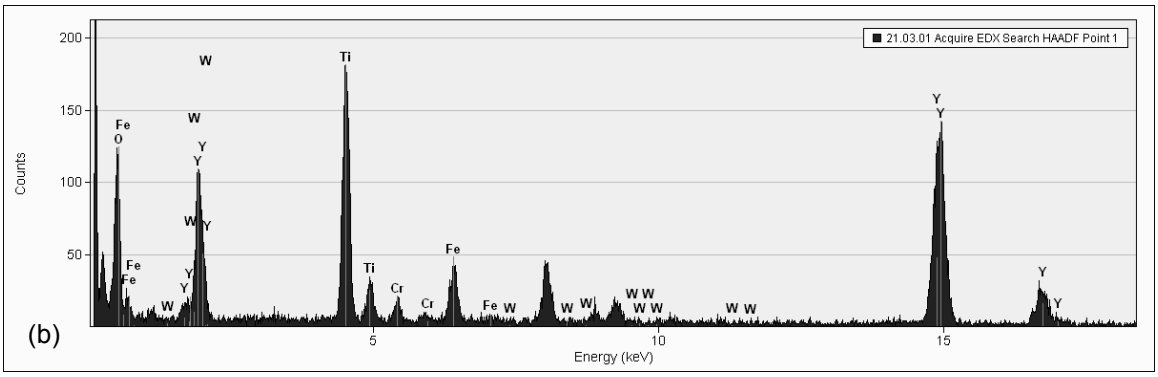
21.03.01 Acquire EDX Search HAADF Point 1
Counts
Energy (keV)
Fe
O
W
Y
Ti
Cr

(c)

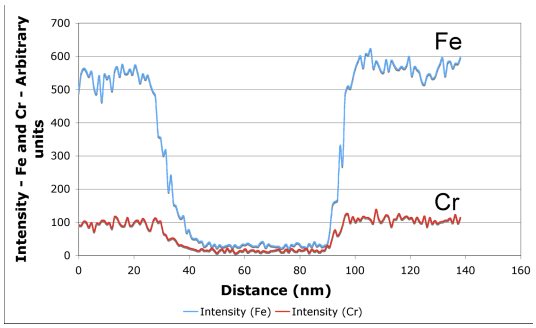
Intensity - Fe and Cr - Arbitrary units
Distance (nm)
Fe
Cr
Intensity (Fe)
Intensity (Cr)

(d)

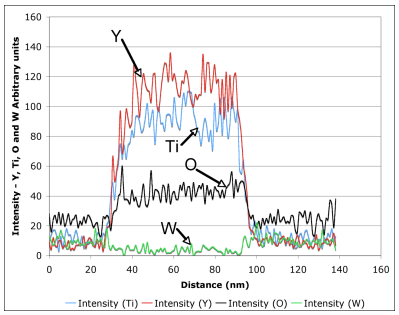
Intensity - Y, Ti, O and W Arbitrary units
Distance (nm)
Y
Ti
O
W
Intensity (Ti)
Intensity (Y)
Intensity (O)
Intensity (W)

(e)

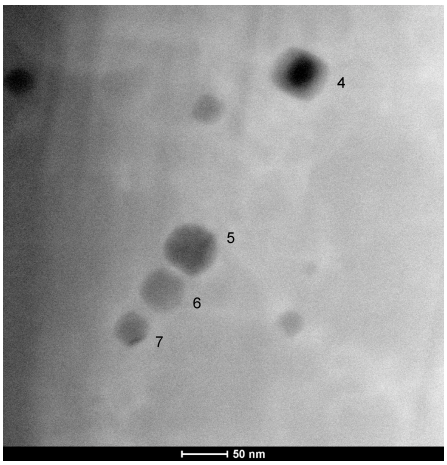
4
5
6
7
50 nm

(f)

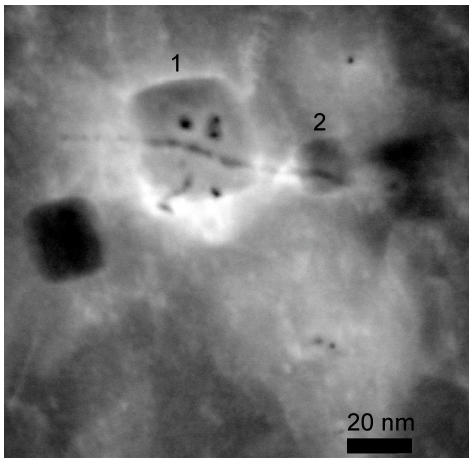

(g)

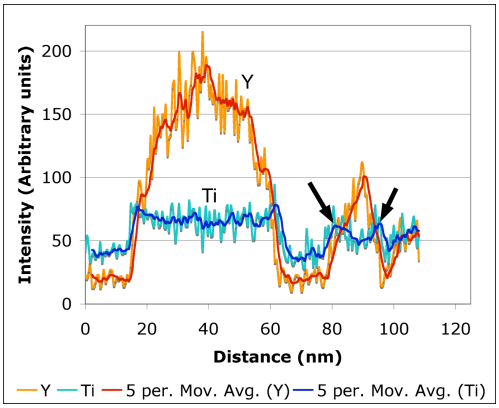

Fig. 5. (a) One of the larger square shaped particles - showing more facets near the corners, (b) EDX spectrum from the same particle, (c) Intensity profile for Fe and Cr across the NF shown in Fig. 5(a), showing sharp concentration drops reaching almost zero inside the NF for both elements, (d) Intensity profile for Ti, Y, O and W showing significant increases in concentration for Ti, Y and O, and a decrease in concentration for W inside the NF, (e) Four different "square" particles in the range of 25-60 nm, (f) two large NFs of different sizes with trace of EDS scan across them (the trace is not straight probably due to sample drift), (g) Ti and Y intensity profiles for particles 1 and 2.

Table 3. Y and Ti concentrations and Y/Ti ratio in intermediate size "square" features (or "large NFs") shown in Fig. 5(e).

	Particle 4	Particle 5	Particle 6	Particle 7
Ti (At. %)	0.6	4.8	3.1	6.3
Y (At. %)	1.1	4.6	2.9	3.9
Y/Ti	1.98	0.96	0.95	0.6

Thus it is clear that the Y/Ti ratio varies substantially from NF to NF. The larger NFs have higher Y/Ti ratio. This is true in general, as also illustrated by an EDS line scan across two NFs of different sizes (marked 1 and 2 in Fig. 5(f)), the Y and Ti intensity profiles for which are given in Fig. 5(g). However, there are some exceptions, such as the NF shown in Fig. 5(a).

It was found from various measurements performed on the micrographs such as those shown in Fig. 4 that these types of NFs with square cross-section have an average volume fraction of approximately 0.4% in the alloy. The density of these precipitates is close to 5 g/cm^3, and that of the matrix approximately 8 gm/cm^3. Assuming that the stoichiometry of the NFs is between Y_2TiO_5 and $Y_2Ti_2O_7$ (as seen from the EDS analysis) the fraction of total Y and Ti present in these NFs can be calculated.

According to these stoichiometries, the weight fraction of Ti in these precipitates is between 0.16 and 0.25, or ~0.2 on average. The total amount of Ti in the alloy is about 0.4 wt %. This will yield a value of approximately 12.5% of the total Ti residing in the square NFs. Similarly, the fraction of Y in the square NFs can be calculated by assuming an average weight fraction of Y in the square precipitates equal to 0.52 (0.58 for Y_2TiO_5 and 0.46 for $Y_2Ti_2O_7$). Since the total amount of Y in the alloy is about 0.2%, the fraction of total Y residing in the square NFs is about 0.65, assuming an average volume fraction of 0.4% for these NFs. The density of the Fe matrix was assumed to be 8 gm/ cm^3 and that of the oxides to be approximately 5 gm/ cm^3 in all of the calculations reported here.

A different region of the sample with similar "square" NFs is shown in Fig. 6(a), indicating the trace of the drift corrected spectrum profile taken from one of the NFs. The plot in Fig. 6(b) shows the profile of Ti, Y and O across the particle. It is clear that the concentration of Y is higher than that of Ti. The concentration of Ti at the edges seems to be slightly higher than that in the center of the NF (as indicated by the arrows). The same effect is seen in the concentration profiles of Fig. 5(g), to some extent (see arrows). This slight core-shell effect was seen in a number of the intermediate sized NFs.

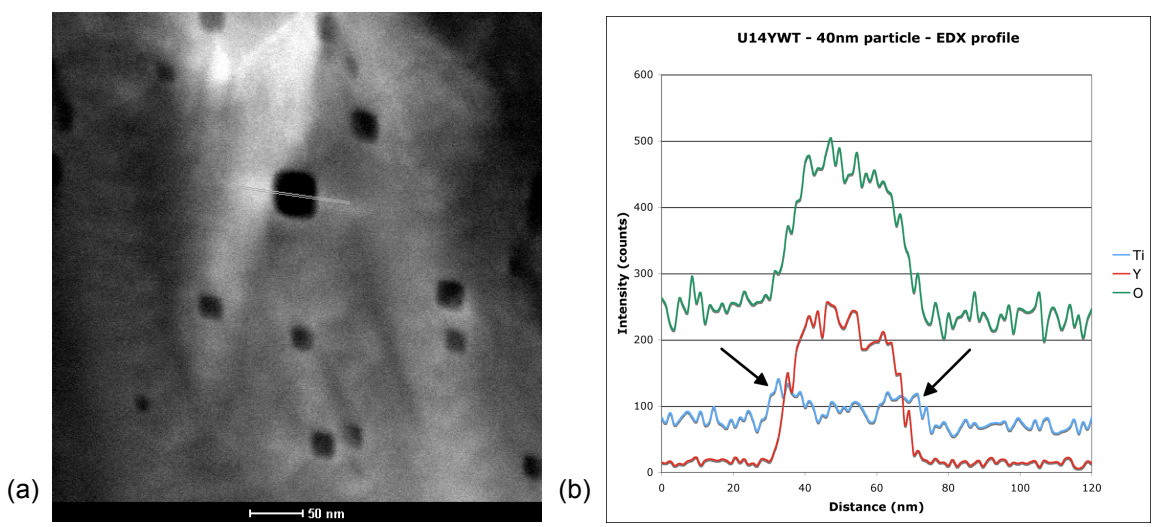

Fig. 6. (a) HAADF STEM image showing a particle across which a drift corrected spectrum profile was taken, (b) The spectrum profiles for Ti, Y and O, showing a high Y/Ti ratio, and a slightly higher Ti amount at the edges of the particle.

The structure of the intermediate sized NFs was investigated using high resolution transmission electron microscopy (HRTEM). An example is shown in Fig. 7(a) for a NF located at a low angle grain boundary in the ferrite (indicated by the arrow). The Y/Ti ratio of the particle was found to be 5/4. The HRTEM image of the particle and the surrounding matrix is shown in Fig. 7(b).

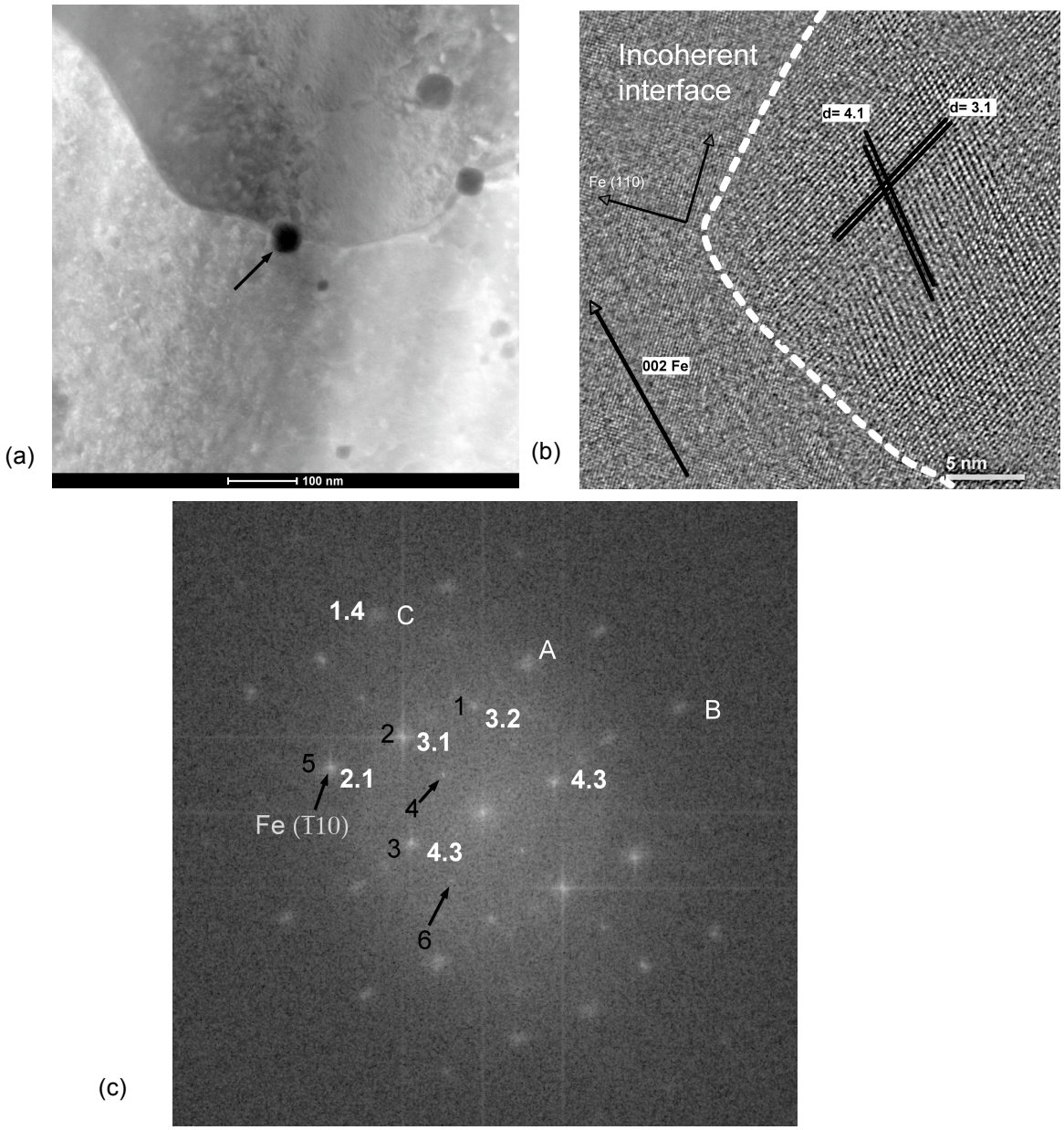

Fig. 7. (a) Particle at a small angle grain boundary, (b) HRTEM image of the "Square" precipitate indicated in (a), showing lattice fringes and the interface between the particle and the matrix, (c) Fast Fourier Transform (FFT) of the HRTEM image in (b) showing both BCC α Fe and precipitate spots.

The interface between the particle and the matrix is indicated by a dashed line. The Fast Fourier Transform (FFT) of this HRTEM image is shown in Fig. 7(c). The spots in the FFT image ware labeled 1 through 5 (black numbers) for the NF and A through C (white letters) for matrix, while the d spacings are shown in white numbers. These spots were analyzed in detail. The spot corresponding to a d-spacing of 2.1Å almost overlaps with the Fe BCC (110) spot. The lattice spacing values and the angles between the lattice planes are shown in Table 4.

Table 4. Measured d-spacing values and angles for the particle shown in Fig. 7.

Image	Spot (a)	d spacing of a (Å)	Spot b	d spacing of b (Å)	θ1 (deg)	θ4 (deg)	Angle between a and b (deg)
Square particle at GB	1	3.2	2	3.1	94.86	137.49	42.63
	2	3.1	3	4.3	137.49	205.11	67.62
	2	3.1	5	2.1	137.49	163.84	26.35
	1	3.2	3	4.3	94.86	205.11	110.25
	4	6.2	3	4.3	137.49	205.11	67.62

Visual examination showed that the d-spacing values and angles between the planes do not match those of any of the known Y-Ti-oxide. The structure of the NF was solved in the following manner. First it was assumed that the NF has a tetragonal structure. This assumption was based on the fact that the FFT pattern from the matrix seems to have 2 mirror planes, and that there is at least one known complex Y-Ti-oxide (Y_2TiO_5) that has a structure that is close to tetragonal. Subsequently, curves from the Hull-Davey chart were used to find the c/a ratio using the known d-spacing values. The c/a ratio was found to be approximately 0.6. The structure was then refined to make the d-spacing values and the angles match the experimentally observed values (from the FFT image) as closely as possible. It was found that the lattice parameters of a=11.6Å, b=12.2Å, and c=7.4Å gave the closest matching between the observed and the calculated d-spacing and angles. Based on these results the lattice was assumed to be face-centered orthorhombic. The corresponding calculated d-spacing values and angles are given in Table 5.

Table 5. Calculated d-spacing values and angles for orthorhombic structure and lattice parameters of a=11.6Å, b=12.2Å and c=7.4Å. The corresponding Miller indices are given in columns 1 and 2.

$h_1k_1l_1$	$h_2k_2l_2$	phi (deg)	d1 (Å)	Corresponding spot in FFT	d2 (Å)	Corresponding spot in FFT
0 -2 2	2 0 2	43.87	3.16	1	3.12	2
2 0 2	2 2 0	67.06	3.12	2	4.20	3
2 0 2	4 2 2	27.92	3.12	2	2.13	5
0 -2 2	2 2 0	110.94	3.16	1	4.20	3

As is clear from a comparison of Tables 4 and 5, there is very good agreement between the measured and calculated d spacing and angles. There are two additional pairs of very faint spots, numbered 4 and 6. These correspond to the precipitate **101** and **12`1** planes. Such spots can be caused by ordering in a direction perpendicular to these

respective planes. This destroys the face-centering of the Bravais lattice and creates a "b centered" lattice.

A simulated diffraction pattern of the NF, using the calculated lattice parameters and a "b-centered" orthorhombic lattice, and that of the matrix, using known a Fe lattice parameters, are shown in Fig. 8 (a) and (b), respectively, reproducing the spots in the FFT (in Fig. 7(c)) as closely as possible. The simulated structure shows ordering on (202) and (24`2) planes. The spots 4 and 6 (corresponding to ±(101) and ±(12`1)) are reproduced at very low intensity, which may be the result of ordering, as was mentioned earlier.

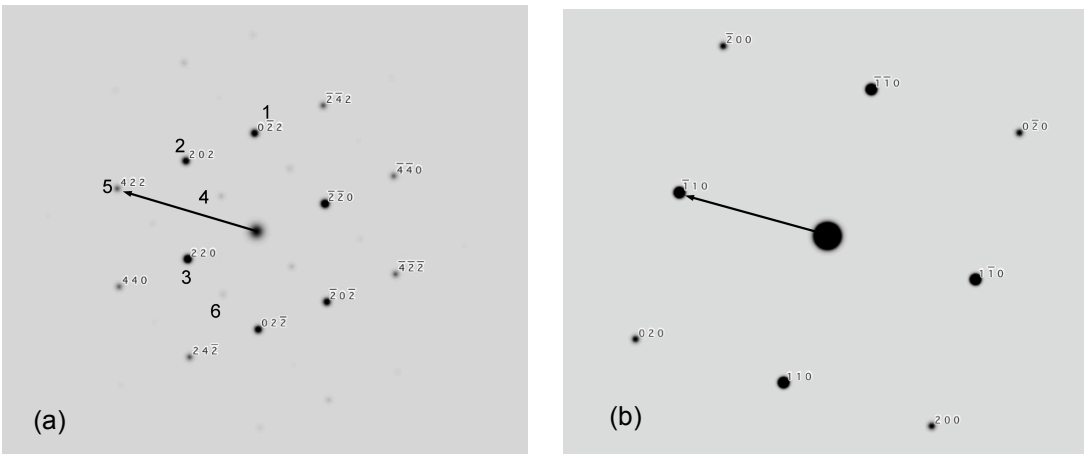

Fig. 8. Simulated diffraction patterns: (a) Precipitate with "**b**-centered" orthorhombic lattice oriented at zone axis $[1\overline{1}\overline{1}]$, (b) Matrix - α Fe oriented at zone axis $[001]$ - the orientation relationship is: (422)ppt || $(\overline{1}10)$Fe matrix; $[1\overline{1}\overline{1}]$ppt || $[001]$ Fe matrix.

The orientation relationship (OR) between the precipitate and the matrix was found to be: (422) ppt || ((`110) Fe Matrix and $[1\overline{1}\overline{1}]$ ppt || [001] Fe matrix.

The HRTEM image from another NF, taken from a different Fe BCC matrix zone axis, also showed fringes which had identical d-spacing values as the one discussed above. The lattice parameters of this structure do not match with those of any known complex Y-Ti-oxides, although they bear some resemblance to orthorhombic Y_2TiO_5, whose lattice parameters are slightly smaller for a (10.35Å) and b (11.25Å), and half for c, which is 3.7Å (see [21]).

The low index matching atomic planes of the precipitate and the matrix ($\{4\ 2\ 2\}_{Precipitate}$ and $\{`1\ 1\ 0\}_{Fe\ BCC}$ planes) are oblique to the interface planes. The lattice mismatch in the $\{`1\ 1\ 0\}_{Fe\ BCC\ \ Fe\ BCC}$ direction is about 7%, and in the direction perpendicular to the plane of the figure it is about 3%, indicating that the interface is probably semi-coherent.

Close examination of the HRTEM image indicates that the interface between the particle and the Fe BCC matrix is irregular, and probably has steps. Such an interface may be developed parallel to some invariant line (of somewhat higher indices) between the two phases [22]. This may cause the formation of steps at the interface, with the terrace planes parallel to the matching low index crystallographic planes.

Small spherical shaped NFs (< 5nm)

The third type of feature in the U14YWT alloy HIP-ed at 1150°C was found to be extremely small, i.e. < 5nm in diameter, as shown in the HRTEM image in Fig. 9(a). The right hand side of the image shows numerous closely spaced spherical NFs, whereas the left hand side of the image shows very few features. This indicates that the NFs are distributed in an inhomogeneous manner inside the a ferrite grain. The average number density of the particles in the matrix, as calculated from this image (Fig. 9(a)), assuming a conservative sample thickness of 100 nm, was found to be ~2 x 10^{23} /m^3. Since the sample is likely to be thinner than 100 nm (since lattice fringes are clearly visible), the NF number density is likely to be higher than this in the grains where the particles are present. This number density is similar to estimates based on small angle neutron scattering (SANS), TEM and APT for similar NFAs [3, 6, 9, 11, 13, 19]. Fig. 9(b) shows an FFT diffraction pattern extracted from the HRTEM image in Fig. 9(a). The spots in the FFT image do not match the patterns for any known Y-Ti-oxides structures.

(a) 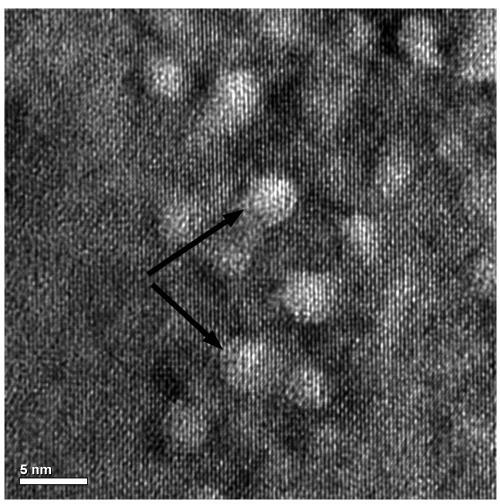

(b) 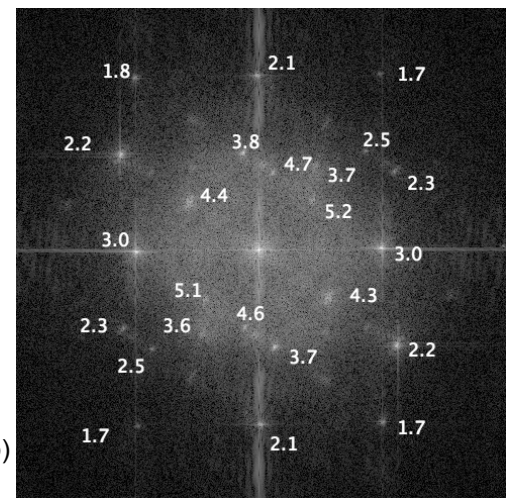

Fig. 9. (a) Extremely small NFs - 2-5nm in size, and spherical in shape as seen in an HRTEM image, (b) An FFT image extracted from HRTEM image in (a), showing reciprocal lattice spots from the NFs.

A U14YWT alloy HIP-ed at 850°C was also examined in the TEM. An HRTEM image, cleaned using a mask filter in the FFT, is shown in Fig. 10(a). The corresponding FFT diffraction pattern is shown in Fig. 10(b).

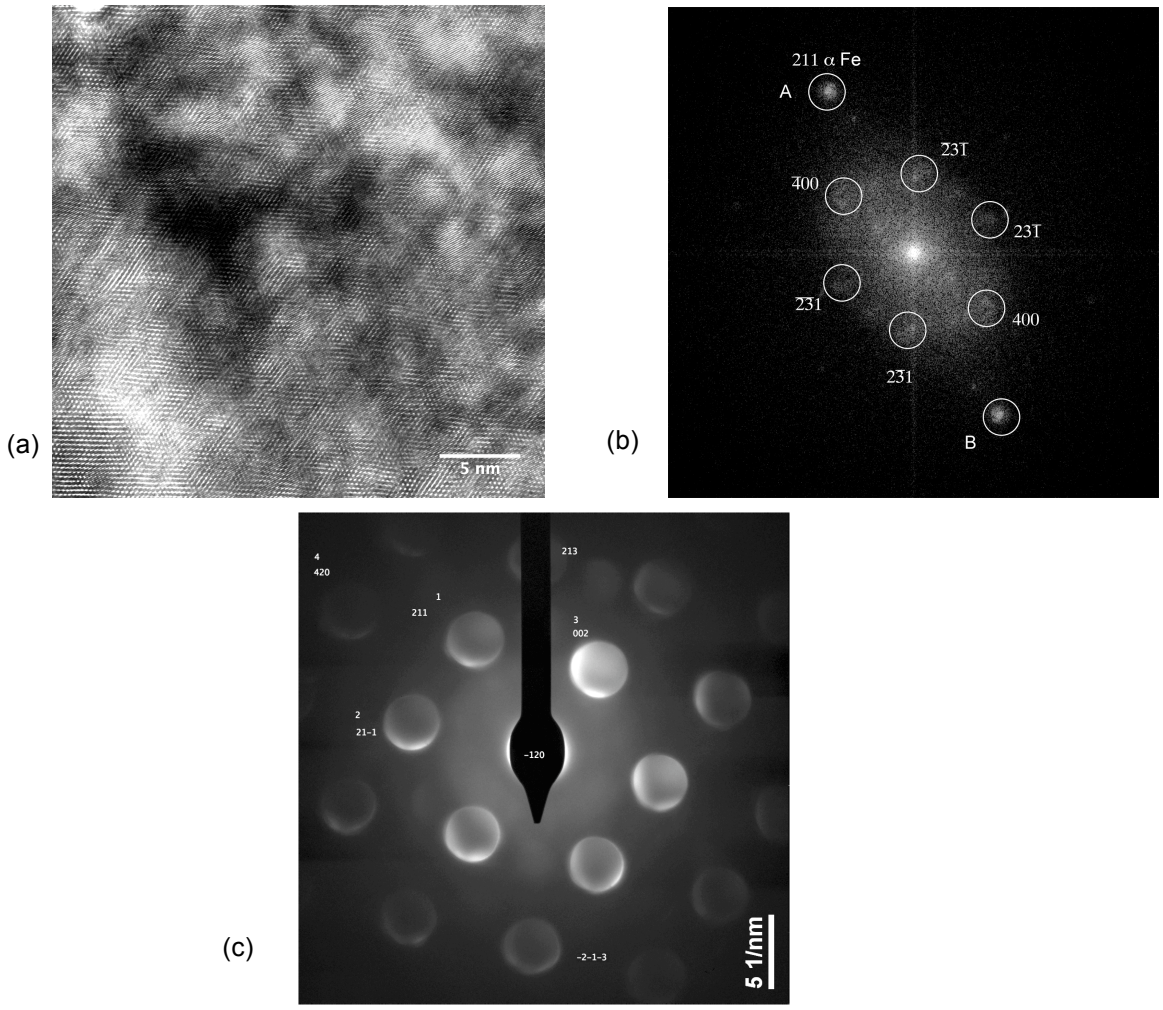

Fig. 10. (a) A cleaned HRTEM image from a U14YWT alloy sample HIP-ed at 850°C, (b) corresponding FFT pattern showing the spots from the Fe BCC matrix and the particles or nano-clusters, (c) Convergent beam electron diffraction pattern from Fe BCC grain whose HRTEM picture is shown in Fig. 10(a).

The spots marked A and B arise from the {211} a Fe planes. The six spots in a hexagonal arrangement are from the NFs, and are consistent with planes in a slightly distorted $Y_2Ti_2O_7$ structure. Using the convergent beam electron diffraction (CBED) pattern in Fig. 10(c), the orientation relationship (OR) between the particles and the matrix was determined to be:
{123} ppt || {123} α Fe and $[30\bar{1}]$ ppt || $[2\bar{1}0]$ α Fe.

Thus there seems to be a difference in the phase of the smallest size NFs found in the U14YWT samples HIP-ed at 1150°C and 850°C, respectively.

DISCUSSION

The microstructure of U14YWT alloy hot isostatic pressed (HIP-ed) at 1150°C was examined using TEM. Three types of features were observed, having different sizes and shapes.

The first type of features, the largest, were present in the size range of 50-300 nm, were irregular in shape, and had facets parallel to low index planes of the BCC iron matrix. They were found to be comprised of Cr, Ti and O, with a solute ratio of ≈ Cr:Ti:O = 1:1:3. Their crystal structure showed d-spacing values which were similar to those reported in literature for a rhombohedral $CrTiO_3$ structure. Due to their low number density, these features are not thought to be important for the radiation damage resistance of U14YWT. Indeed, they may have a slight detrimental effect on the properties of the alloy as they may remove a significant amount of Ti from the surrounding matrix, thus preventing the formation of the beneficial NFs.

The second type of feature, in the size range of 10-50 nm, were polyhedral, with faceted or rounded corners and an approximately square center section. These intermediate sized precipitates are classified here as "larger NFs". EDS showed the larger NFs were primarily composed of Y, Ti and O. The Y:Ti ratio varied from NF to NF in the range of <1:1 to ~2:1. The edges of these particles seem to have more Ti than at the center, suggesting a possible core-shell structure. Similar core shell structures have been observed previously in NFs present in other NFAs [23]. The larger NFs seemed to have slightly higher Y:Ti ratio. This observation may suggest that for the larger NFs, there is greater opportunity to reach an equilibrium composition, which may have a high Y:Ti ratio. Similar variations in Y:Ti ratio with size have also been observed in a sample of MA-957 alloy steel, although only up to a size range of ~15-20 nm, after which the authors reported a roughly constant Y:Ti ratio [24].

The structure of these larger NFs was examined using high-resolution TEM. A detailed examination of HRTEM micrographs and their FFT images suggested an orthorhombic phase, with the lattice being centered on one of the faces. The lattice parameters were found to be a= 11.6Å, b= 12.2Å and c= 7.4Å. The two larger parameters, a and b, were close to the lattice parameters of orthorhombic $Y_2Ti_2O_5$, and the third parameter, c, was found to be double that of the c edge of Y_2TiO_5. The spots in the FFT pattern of the HRTEM image suggested that there was ordering on two oblique planes. These larger NFs do not have a structure that is identical to any of the known Y-Ti-oxides, although it is somewhat similar to the orthorhombic Y_2TiO_5 phase. They also exhibit a variable, non-stoichiometric composition. These observations suggest that the larger NFs are not at equilibrium, but belong to a metastable transition phase. The high- resolution TEM images suggested that the interface between these particles and the Fe BCC matrix was irregular, and possibly stepped. The interface was observed to be semi-coherent, which may act as good sinks for defects and help in the trapping of He, thus preventing the formation of large bubbles in the neighboring matrix. These NFs are different from those reported in other studies by Hoelzer, Miller et al. [9, 13] in that they have a nominally square cross-section, are quite well distributed in space for their size range, and their structure is not identical to any known Y-Ti-oxide.

These NFs appear in very high number densities ($2x10^{20}$ – $7x10^{20}$ / m^3), and thus provide significant surface area per unit volume for He entrapment. The ability of larger NFs (similar in size as reported here) to trap inert gases such as Ar is exemplified by the existence of cavities filled by Ar decorating the interface between the matrix and the particle in the work of Klimiankou, et al. [18] The average distance between these particles is ~90-100 nm. Such small distances between these NFs can result in significant increase in strength by providing resistance to dislocation motion. Thus, although these NFs are larger than the 2-5nm NFs generally thought to be the primary

reason for enhanced radiation resistance and strength, they are present in substantially small sizes and number densities to affect the properties of the alloy significantly. Moreover, their presence also diminishes the concentration of available solute elements for the precipitation of the smaller NFs, and as much as ~12-15% of Ti and ~ 60-70% of Y may reside in these square NFs. Therefore, it is of extreme interest to the NFA community to understand if these larger particles can compensate for the lower concentration of the 2-5 nm NFs.

A third type of small NFs, less than 5nm in diameter, were distributed in the Fe BCC matrix inhomogeneously. Some of the grains showed a high number density of these precipitates, while some others did not have detectable numbers. The number density of these particles was estimated to be of the order of $2x10^{23}$ particles/m^3 in the regions in which they were observed. This number is close to that estimated by SANS and 3-DAP in the same 14YWT alloy and in similar alloys. High-resolution TEM (HRTEM) images and corresponding FFT images were not consistent with the structure of known Y-Ti-oxides. This was found to be in contrast to the extremely tiny clusters that were found in the U14YWT alloy HIP-ed at 850°C, which may be $Y_2Ti_2O_7$. The exact nature of the small NFs (<5 nm) needs to be investigated further using extraction of these precipitates from the alloy using a carbon replica method [25-26].

The inhomogeneous distribution of the small NFs (<5nm) and the significant number of the larger NFs (5-10nm) makes the understanding of the effects of the larger NFs on the properties of these steels important for the development of these alloys.

ACKNOWLEDGEMENTS

The corresponding author dhriti1@gmail.com is at the Institute of Materials Engineering, ANSTO, NSW, Australia, 2234. The authors would like to thank Dr. Longzhou Ma at UNLV for his kind permission to use the TEM at the Harry Reid Environmental Center when needed. The many helpful discussions with Prof. J. P. Hirth are also gratefully acknowledged. This TEM work at LANL was funded by Los Alamos National Laboratory LDRD. The alloy development and characterization studies carried out at UCSB were supported by the DOE Offices of Fusion Energy Sciences and Nuclear Energy.

REFERENCES

[1] S. J. Zinkle, Busby, J. T., "Structural Materials for Fission and Fusion Energy," *Mater. Today* 2009, 12:12.

[2] M. I. Hoffert, Caldeira, K., Benford, G., Criswell, D. R., Green, C., Herzog, H., Jain, A.K., Kheshgi, H. S., Lackner, K.S., Lewis, J. S., Lightfoot, H. D., Manheimer, W, Mankins, J. C., Mauel, M. E., Perkins, L. J., Schlesinger, M. E., Volk, T., Wigley, T. M. L., "Advanced Technology Paths to Global Climate Stability: Energy for a Greenhouse Planet," *Science* 2002, 298:981.

[3] Odette, G. R., Alinger, M. J., Wirth, B. D., "Recent Developments in Irradiation-Resistant Steels," *Annu. Rev. Mater. Res.* 2008, 471.

[4] Mansur, L. K., "Theory and Experimental Background on Dimensional Changes in Irradiated Alloys," *J. Nucl. Mater.* 1994, 216:97.

[5] Czyrska-Filemonowicz, A., Dubiel, B., "Mechanically Alloyed, Ferritic Oxide Dispersion Strengthened Alloys: Structure and Properties," *J. Mater. Process. Tech.* 1997, 64:53.

[6] Odette, G. R., Hoelzer, D. T., "Recent Progress in Developing Irradiation Tolerant Nanostructured Ferritic Alloys: Transforming Helium Accumulation from a Liability to an Asset," JOM Journal of the Minerals, Metals and Materials Society 2010, In Press.

[7] Yamamoto, T., Odette, G. R., Miao, P., Edwards, D.J., Kurtz, R.J., "Helium Effects on Microstructural Evolution in Tempered Martensitic Steels: In situ Helium Implanter Studies in HFIR," *J. Nucl. Mater.* 2009, 386-388:338.

[8] Odette, G. R., Miao, P., Edwards, D. J., "Helium Transport, Fate and Management in Nanostructured Ferritic Alloys: In Situ Helium Implanter Studies," *J. Nucl. Mater.* 2010, accepted for publication.

[9] Hoelzer, D. T, Bentley, J., Sokolov, M. A., Miller, M.K., Odette, G. R., Alinger, M.J., "Influence of Particle Dispersions on the High-Temperature Strength of Ferritic Alloys," *J. Nucl. Mater.* 2007, 367-370:166.

[10] Miller, M. K., Hoelzer, D. T., Kenik, E. A., Russell, K. F., "Stability of Ferritic MA/ODS Alloys at High Temperatures," *Intermetallics* 2005, 13:387.

[11] Alinger, M. J., Odette, G. R., Hoelzer, D. T., "On the Role of Alloy Composition and Processing Parameters in Nanocluster Formation and Dispersion Strengthening in Nanostuctured Ferritic Alloys," *Acta Mater.* 2009, 57:392.

[12] Miller, M. K., Hoelzer, D. T., Kenik, E. A., Russell, K. F., "Nanometer Scale Precipitation in Ferritic MA/ODS Alloy MA957," *J. Nucl. Mater.* 2004, 329-333:338.

[13] Miller, M. K., Russell, K. F., Hoezler, D. T., "Characterization of Precipitates in MA/ODS Ferritic Steels," *J. Nucl. Mater.* 2006, 351:261.

[14] Bai, X-M., Voter, A. F., Hoagland, R. G., Nastasi, M., Uberuaga, B. P., "Efficient Annealing of Radiation Damage Near Grain Boundaries via Interstitial Emission," *Science*, 327:1631.

[15] Demkowicz, M. J., Hoagland, R. G., Hirth, J. P., "Interface Structure and Radiation Damage Resistance in Cu-Nb Multilayer Nanocomposites," *Phy. Rev. Lett.* 2008, 100:136102.

[16] Misra, A., Demkowicz, M., Zhang, X., Hoagland, R., "The Radiation Damage Tolerance of Ultra-High Strength Nanolayered Composites," *JOM J. Minerals, Metals and Mater. Soc.* 2007, 59:62.

[17] Klimiankou, M., Lindau, R. M. A., "TEM Characterization of Structure and Composition of Nanosized ODS Particles in Reduced Activation Ferritic-Martensitic Steels," *J. Nucl. Mater.* 2004, 329-333:347.

[18] Klimiankou, M., Lindau, R. M. A., "Energy-Filtered TEM Imaging and EELS Study of ODS Particles and Argon-Filled Cavities in Ferritic-Martensitic Steels," *Micron* 2005, 36:1.

[19] Alinger, M. J., Materials Engineering, vol. Ph. D. Santa Barbara: University of California, Santa Barbara, 2004.

[20] Vasyutinski, N., "Ryseva," *Russ. J. Inorg. Chem.* 1978, 23:621.

[21] Mumme, W. G., Wadsley, A. D., "The Structure of Orthorhombie Y2TiO5, an Example of Mixed Seven and Fivefold Coordination," *Acta Crystallogr.* 1968, B24:1327.

[22] Furuhara, T., Howe, J. M., Aaronson, H. I., "Interphase Boundary Structures of Intragranular Proeutectoid Alpha-Plates in a Hypoeutectoid Ti-Cr Alloy," *Acta Metall. Mater.* 1991, 39:2873.

[23] Marquis, E. A., "Core/Shell Structures of Oxygen-Rich Nanofeatures in Oxide-Dispersion Strengthened Fe--Cr Alloys," *Appl. Phy. Lett.* 2008, 93:181904.

[24] Sakasegawa, H., Chaffron, L., Legendre, F., Boulanger, L., Cozzika, T., Brocq, M., de Carlan, Y., "Correlation Between Chemical Composition and Size of Very Small Oxide Particles in the MA957 ODS Ferritic Alloy," *J. Nucl. Mater.* 2009, 384:115.

[25] Czyrska-Filemonowicz, A., Gorczyca, S. S. K., "Extraction Double-Replica Technique for Electron Microscopy Studies of Precipitates," *Prakt. Metallogr.* 1992, 29:35.

[26] Egeland, G. W., Zhang, H., Wang, H., Dai, Y., "Precipitate Analysis of 9-12 % Cr Ferritic/Martensitic and ODS Steels Using the Carbon Replica Technique," International Conference on Fusion Reactor Materials - ICFRM-13. Nice, France, 2007.